INORGANIC CHEMISTRY
FRONTIERS

REVIEW

View Article Online
View Journal | View Issue

Cite this: *Inorg. Chem. Front.*, 2020, **7**, 28

Recent progress in pyrolyzed carbon materials as electrocatalysts for the oxygen reduction reaction

Chen Ouyang and Xun Wang *

The oxygen reduction reaction (ORR) is an important reaction in fuel cells. The efficiency of the ORR is related to the efficiency of fuel cells. Therefore, research on ORR catalysts is an essential issue. Non-precious metal catalysts (NPMCs) have been a research hotspot in recent years due to cost considerations, and carbon-based catalysts are an important component of NPMCs. Carbon-based catalysts have a wide range of sources, are low-cost, and have superior performance and good stability. In this review, the pyrolysis step in the preparation of carbon-based catalysts was utilized to analyze the composition of the pyrolysis precursor and the effect of the structure on the catalytic activity of the catalyst. We classify carbon-based catalysts into four types depending on the type of precursor: biomass-derived, organic mixture-derived, MOF-derived, and molded carbon material-derived carbon-based catalyst. At the same time, the influence of pyrolysis conditions on the catalytic activity of the product was considered.

Received 31st July 2019,
Accepted 24th October 2019

DOI: 10.1039/c9qi00962k

rsc.li/frontiers-inorganic

1. Introduction

Since the industrial revolution, the energy issue has been the focus of scientific research, and fuel cells are an energy conversion technology that has received widespread attention for decades.[1–3] They have the characteristics of a high energy conversion rate and low carbon emission, which can effectively alleviate the contradiction between increasing energy demand and environmental protection.[4] However, the application of fuel cells is affected by cost and performance, because Pt-based catalysts used in conventional fuel cells are relatively expensive, accounting for about 20% of the total cost of fuel cells. At the same time, the oxygen reduction reaction (ORR) of the cathode in the fuel cell occurs with more difficulty than the oxidation reaction of the anode, and about 80% of the catalyst is supported at the cathode for catalyzing the slow ORR.[5] In addition, the long-term stability, anti-CO and methanol toxicity of Pt-based catalysts are poor. On the one hand, researchers are trying to reform precious metal catalysts to reduce the cost, improve performance, and improve stability. Liu *et al.*[6] used ZIF pyrolysis products to support platinum, followed by secondary pyrolysis to obtain a PtCo alloy catalyst with excellent performance. On the other hand, the development of a catalyst which is inexpensive and does not have the above disadvantages is an ideal solution for solving the problem of fuel cell application, namely development of non-precious metal catalysts (NPMCs)[7–10]

When developing catalysts, we must consider factors such as catalytic activity, conductivity, price, and stability.[11,12] Conventional noble metal catalysts excel in catalytic activity and electrical conductivity, but their stability is poor.[13] Oxide catalysts have good stability and low price, but their activity and conductivity are unsatisfactory.[14] In the research process, researchers often use carbon materials as load materials.[15] Carbon materials have good electrical conductivity and stability; at the same time, they are inexpensive.[16] It is only necessary to load a catalytically active material onto a carbon material to obtain a catalyst having excellent catalytic performance. Among them, a nanoporous carbon structure containing a large number of pores,[17] which can effectively improve the load ratio, is a good choice as a load material.

Nanoporous carbon is produced by pyrolysis of carbonaceous organic matter; pyrolysis is thermochemical decomposition of organic materials at elevated temperatures in the absence of oxygen,[18] involving the concurrent transformation of the chemical composition and physical phase, and is irreversible. Pyrolysis differs from other high-temperature processes like combustion and hydrolysis in that it usually does not result in reactions with oxygen, water, or any other reagents. Researchers found that when using a precursor containing a transition metal ion or a heteroatom for pyrolysis, the resulting nanoporous carbon itself has ORR catalytic activity,[19] these have been called carbon-based catalysts.[20] Carbon-based catalysts are low cost, and have good electrical conductivity and excellent stability. The catalytic activity of the catalyst is generally determined by the type, amount and extent of exposure of the active site.[5] The type of active site of carbon-based catalysts is influenced by precursors and pyrol-

Key Lab of Organic Optoelectronics and Molecular Engineering, Department of Chemistry, Tsinghua University, Beijing 100084, China.
E-mail: wangxun@mail.tsinghua.edu.cn

ysis conditions.[21] Researchers have proposed many strategies to adjust the electronic structure of the carbon surface to effectively enhance the intrinsic activity of the catalyst.[22] The number of active sites can be increased by modifying the doping ratio of the precursor. Similarly, we can control the geometry of the carbon catalyst to adjust the active site more effectively by adjusting the composition of the precursor and the pyrolysis conditions.[23]

Several excellent review articles have summarized the progress of the carbon-based ORR catalysts achieved during the past few years,[5,24–27] which well covered the synthesis routes and the structure construction. To avoid duplicating the published work, this review will focus on some research progress of carbon-based catalysts that obtain different active sites by pyrolysis of different types of precursors under different conditions, and try to understand the process of pyrolysis of carbon-based catalysts from different perspectives.

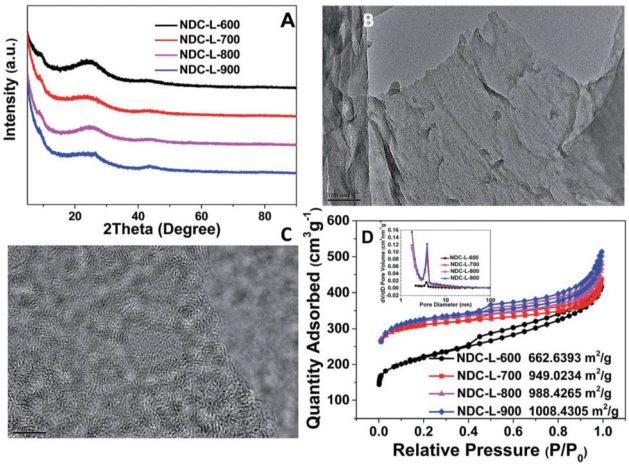

Fig. 1 (A) XRD pattern over the 2θ range of 5–90° of NDC-L-600, NDC-L-700, NDC-L-800, and NDC-L-900. (B) TEM and (C) HRTEM images of NDC-L-800. (D) N_2 adsorption–desorption isotherms of NDC-L-700, NDC-L-800, and NDC-L-900. The inset is pore-size distributions (PSDs) of the four samples.

2. Biomass-derived carbon-based catalyst

The method of preparing carbon materials by incomplete combustion of biomass appeared in the early days of human civilization, and pyrolysis can be regarded as an extremely incomplete combustion process. The global annual biomass production is more than 2×10^{11} tons (dry carbon basis) as estimated in 2016.[28] These biomass sources are broad, diverse, and rich in composition.[29] The main components include cellulose, hemicellulose, and lignin. Biomass is heated to a medium temperature (generally 300–500 °C) without oxygen or a limited supply of oxygen to obtain biological oils, gases and biochar, so that the directly obtained biochar has a small specific surface area due to the presence of bio-oil and the like, and the pore quality is poor. So the catalytic performance of the biomass-derived carbon-based catalyst (bio-carbon) is generally improved by increasing the pyrolysis temperature or by activating before use. Compared with activated carbon and carbon black derived from fossil fuel, bio-carbon has more surface functional groups and nanostructures, and thus may lead to better catalytic activity.[30]

For ORRs, N, S, P heteroatom-rich biomass is an excellent precursor for the production of heteroatom-doped carbon materials that can be utilized directly as high-efficiency ORR catalysts. Among them, the most commonly known is the nitrogen-doped bio-carbon ORR catalyst. Gao *et al.*[31] directly subjected amaranth waste to high temperature pyrolysis under a N_2 atmosphere to obtain amorphous nitrogen-doped carbon (NDC) with equivalent ORR catalytic activity to commercial Pt/C. TEM images (Fig. 1B and C) show that the NDC consists of randomly stacked graphite-like planar layers, and its highly disordered structure brings high porosity and a large specific surface area. The pore size distribution calculated by the Barrett–Joyner–Halenda (BJH) method ranges from 0.5 to 4.0 nm. The specific surface areas of NDC-L-700, NDC-L-800, and NDC-L-900 (Fig. 1D) were 949.02, 988.43 and 1008.43 $m^2\ g^{-1}$, respectively. The linear sweep voltammetry (LSV) measurement was performed in 0.1 M KOH. The initial potential (0.27 V) and the limiting current density (-4.38 mA cm^{-2}) of NDC-L-800 were very close to those of commercial Pt/C (0.30 V, -4.66 mA cm^{-2}). The authors attribute this excellent performance to the adsorption of oxygen molecules on the carbon surface promoted by the electronegativity difference between the heavily doped pyridine N and the carbon atoms of the carbon material. This statement is corroborated by XPS characterization results.

For most biomass, it is necessary to introduce a nitrogen source during pyrolysis in order to increase the nitrogen doping amount of the carbon material obtained by pyrolysis. Ammonia gas is used extensively as a common nitrogen source in industrial and agricultural production. Pan *et al.*[32] carried out pyrolysis of Ginkgo biloba leaves at 1000 °C for 5 hours under an Ar atmosphere, washing and drying, and further treatment under an ammonia atmosphere at 1000 °C for 5 hours to obtain nitrogen-doped porous carbon nanosheets. The material has an extremely high specific surface area (1436.02 $m^2\ g^{-1}$) and excellent ORR catalytic activity, and its limiting current density and half-wave potential in an alkaline solution are very similar to those of Pt/C.

Ammonia gas has certain toxicity and is flammable. Urea can decompose at high temperature to produce ammonia gas. Therefore, urea can play the same role as an ammonia atmosphere, and it is safer. Liu *et al.*[33] developed an extremely simple method for the preparation of nitrogen-doped porous carbon by direct pyrolysis of cellulose nanocrystals and urea without involving any catalysts and after treatment. The obtained nitrogen-doped porous carbon nanosheet has excellent ORR catalytic performance. It is worth noting that when we add $FeCl_3$ to the system or replace urea with ammonia as the nitrogen source, the obtained material performance

deteriorates, indicating that urea in this preparation process has a unique role rather than simply as a source of ammonia gas generation.

There are many other methods for preparing nitrogen-doped nanoporous carbon by pyrolysis using other nitrogen sources. M. Graglia *et al.*[34] developed a method for introducing nitrogen by nitrating biomass (Fig. 2). Taking lignin as an example, the lignin is first subjected to aromatic nitration to obtain nitro lignin, which is then reduced to amino lignin. The amino lignin and $KCl/ZnCl_2$ mixed salt are co-pyrolysis to obtain nitrogen-doped nanoporous carbon.

In addition to N, carbon materials doped with other heteroatoms such as S, P, O, and B also have a certain ORR catalytic activity. Zhao Lei[35] directly pyrolyzed Pulsatilla chinensis (Bunge) Regel at 1000 °C to obtain a P-doped honeycomb carbon material. Gao *et al.*[36] reported a porous 3D structure of N, S co-doped biochar obtained by pyrolysis of honeysuckle. The carbon structure of the 3D crosslinked network with abundant macropores is obtained by simple pyrolysis and acid etching, and also contains well-doped N and S atoms. The synthesized material exhibited excellent ORR activity, resistance to methanol and stability in 0.1 M KOH solution. Such excellent ORR performance can be attributed to the synergistic effect, including a high number of ORR catalytic sites due to the S, N doping, favorable reactant transport channels provided by the pore structures, and the fast electron transfer rate induced by the continuous 3D networks.

In addition to the ORR catalytically active sites formed by the heteroatoms such as N, P, S, and B, metal-related active sites are also widely studied. Fe, Ni, Co and other elements are widely present in the Earth's crust, and their addition can effectively increase the ORR catalytic activity of porous carbon without excessively improving the cost. Wan *et al.*[37] reported N, P and Fe-tridoped nanoporous carbon ORR catalysts derived from plant biomass corn silk. They first carbonized biomass through hydrothermal methods and then pyrolyzed it under a NH_3 atmosphere at 850 °C, followed by further pyrolysis with $FeCl_3$ to obtain a N–P–Fe–C catalyst. The synergistic effect of N and Fe introduced during the pyrolysis process greatly enhanced the ORR activity, and similar phenomena were observed in some other studies. Pd nanoparticles supported on N-doped carbon from biomass have been reported to exhibit favorable electrochemical activity for the ORR with high catalytic performance and long-term stability.

The ORR catalytic performance of most pyrolyzed biochar materials is comparable to that of 20% Pt/C; although their performance in fuel cells is slightly worse than that of 20% Pt/C, their wide range of low-cost features still brings certain application prospects.

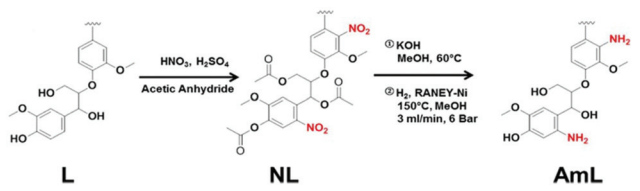

Fig. 2 Synthetic pathway for the conversion of alkali-lignin (L) into aminated lignin (AmL) *via* aromatic nitration.

3. Organic mixture-derived carbon-based catalyst

Biomass-based pyrolytic carbon materials are widely available at low cost; however their performance is constrained by the structure and composition of the precursor biomass, sometimes the desired pyrolysis results are not obtained. At the same time, the biomass composition is complex, and the presence of some impurities is necessary to post-treat the pyrolysis products, sometimes causing uncontrollable effects on the pyrolysis products.[38] Therefore, on the basis of biomass pyrolysis, the researchers have prepared a series of organic pyrolytic carbon materials with excellent ORR catalytic activity by regulating the composition and structure of organic precursors.

Small molecule organic matter is therefore difficult to form a carbon material with a stable structure during pyrolysis; therefore, first consider the pyrolysis of macromolecular organic matter. Wang *et al.*[39] used a nitrogen-rich vitamin B5 as a nitrogen source to easily obtain a nitrogen-doped carbon network (CN) by pyrolysis (700–1000 °C) under an Ar atmosphere. The porous structure and the graphite carbon lattice can be seen in the SEM and TEM images, respectively, which are beneficial to the electrochemical activity of the material: macropores act as ion-buffering reservoirs, the mesopores serve as channels for the rapid transport of ions, while the micropores are the locations for the charge accommodation in the double electrical layer. The results of the LSV measurement (Fig. 3b) show that the ORR activity of CN-700 and CN-800 is stronger than that of CN-900 and CN-1000, and the XPS measurement (Fig. 3a) shows the decrease of N content and the conversion of pyrrole nitrogen to graphite nitrogen indicates that the nitrogen content and nitrogen group in the nitrogen-doped carbon network are important factors for improving the electrocatalytic activity. The nitrogen-doped carbon network also exhibits excellent stability and resistance to methanol toxicity.

Cao *et al.*[40] used cation exchange resin D113 as a precursor to pyrolyze at 1100 °C under different conditions to obtain

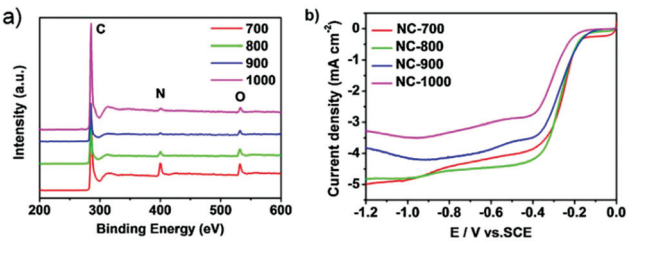

Fig. 3 (a) XPS survey for ultrathin N-doped carbon nanosheet networks, (b) RDE voltammograms of CN-700, CN-800, CN-900 and CN-1000 in an O_2-saturated 0.1 M aqueous KOH solution with a scan rate of 10 mV s^{-1} at 1600 rpm.

different carbon materials, including the Ar atmosphere (D113), NH_3 atmosphere (D113/N), and pre-exchange of $FeCl_2$ (Fe/C), and pre-exchange of $FeCl_2$ & use of the NH_3 atmosphere (Fe/N/C). From the TEM image we can observe that D113/N consists of amorphous carbon flakes, while Fe/N/C contains highly graphitized carbon bands, which indicates the catalytic effect of Fe ions on graphitization during pyrolysis. XPS results show that the nitrogen content in Fe/N/C (0.57 at%) is less than the nitrogen content in D113/N (1.22 at%), indicating that NH_3 is easier to etch amorphous carbon than graphite carbon. At the same time, ORR catalytic activity increased according to the order of D113, Fe/C, Fe/N/C and D113/N, indicating that N-doping can effectively enhance the ORR catalytic activity, and graphitization does not necessarily enhance the catalytic activity of carbon materials.

The scheme of direct pyrolysis of organic macromolecules is simple and convenient, but the composition of organic macromolecules is relatively fixed, and sometimes the microstructure and doping ratio we want cannot be obtained; the pyrolysis of the organic mixture then becomes the next research object. Li *et al.*[41] synthesized N, S double doped graphene nanosheets by pyrolysis of a mixture of melamine and dibenzyl sulfide. Graphene nanosheets with different structures and doping ratios can be prepared by adjusting the ratio of melamine to dibenzyl sulfide. The XPS results show that the proportion of each element in the pyrolysis product is positively correlated with the proportion of elements in the precursor, and the different doping ratios of the graphene nanosheets also showed different ORR properties. The LSV measurement results (Fig. 4a) in 0.1 M KOH showed that the ORR performance was the best when the molar ratio of melamine to dibenzyl sulfide was 6 : 1 ($E_{1/2}$ = 0.83 V *vs.* RHE). The appropriate exposure of S/N is critical to the enhanced ORR process. The results (Fig. 4b) reveal that the doping effect on the ORR is heavily dependent on the synergistic effect of S and N atoms in S, N dual-doped carbon materials.

A prominent problem with the pyrolysis of organic mixtures is that sometimes it is not possible to obtain a catalytically favorable microstructure, such as the previously described mixed melamine and dibenzyl sulfide pyrolysis scheme, when the molar ratio of the two is 1 : 1, an amorphous carbon material is obtained, which may adversely affect the catalytic activity. The intuitive solution to this problem is to use a template method in which a thermally stable porous material is

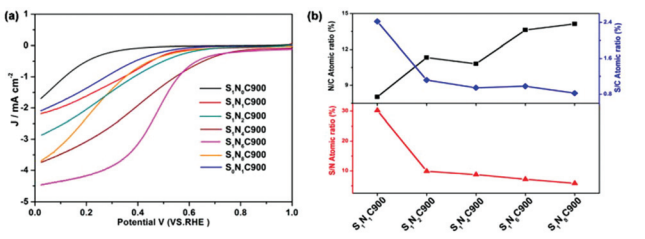

Fig. 4 (a) LSV curves of S_xN_yC900 samples in O_2-saturated 0.5 M H_2SO_4 aqueous solution. (b) N/C, S/C, and S/N atomic ratios.

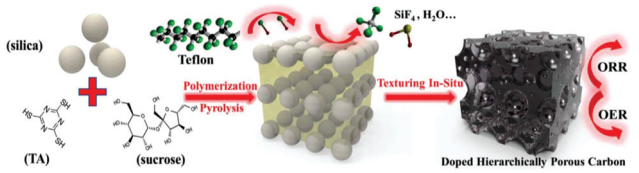

Fig. 5 Illustration of the one-pot fabrication process of doped porous carbon materials. The sucrose and TA precursors were polymerized in the presence of silica followed by Teflon addition. The mixture was pyrolyzed to allow an *in situ* texturing process, which resulted in N, S as well as O enriched, hierarchically micro-, meso-, and macroporous carbon catalysts.

added to the organic mixture precursor as a template, and a nanoporous carbon having regular pores can be obtained by a template effect in the pyrolysis process, which is also called a hard template method. A typical solution is that of Atanassov *et al.*[42] who pyrolyzed the silica, ferric nitrate, and carbendazim mixture precursors, followed by etching, and finally obtained a "self-supported" open frame morphology catalyst. Evaluation of these new catalysts in single membrane electrode assembly has shown an exceptionally high open circuit voltage of 1 V. However, such methods require the removal of the template after pyrolysis. This requires the use of HF, which is extremely harmful to the environment and human body. Pei *et al.*[43] embedded silica spheres in a precursor mixture of sucrose and trithiocyanuric acid (Fig. 5), and then mixed them with Teflon powder for pyrolysis, and Teflon powder decomposes at high temperature to produce HF *in situ* etched SiO_2 to obtain N, S-doped graded porous carbon.

The thermogravimetric analysis shows that the silica template is completely removed during the pyrolysis process. The obtained carbon material contains macropores of about 90 nm and mesopores of about 11 nm. And a large number of micropores and the macropores are from the silica template, and the mesopores and micropores may come from small molecules generated during pyrolysis of organic matter. The graded porous structure and abundant doping heteroatoms bring excellent ORR activity to the material and afforded an onset potential of 0.99 V (0.88 V) and an $E_{1/2}$ of 0.85/0.88 V (0.73 V) in 0.1 M KOH ($HClO_4$) solution. In addition, zinc salts can be added to the precursor, and the carbon produced during the pyrolysis will reduce the zinc ion to metal zinc, and then, due to the lower boiling point of zinc, it is carried away by the protective gas, leaving pores.

Similarly, P. Bogdanoff *et al.*[44] used oxalate as a blowing agent to obtain more finely dispersed and smaller catalytic particles.

4. MOF derived carbon-based catalyst

Metal–organic frameworks (MOFs) are compounds consisting of metal ions or clusters coordinated with organic molecules, which have cosmetic well defined pores with diameters ranging from 0 (nonporous) to 9.8 nm, so we can convert MOFs into carbon/metal porous materials by pyrolysis.[45] The

MOF derived carbon inherited characters of pristine MOFs to a large degree, such as a large surface area, composition diversity and dispersion, tailored porosity.[46,47]

Compared with traditional nanoporous carbon materials, MOFs have many unique advantages as precursors.[48] The main points are as follows: (1) simple preparation methods, (2) ordered and controllable porous structures, (3) high specific surface area, and (4) they easily dope highly dispersed heteroatoms. One of the pioneering studies was that Ma *et al.*[49] used ZIF-67 as a precursor to synthesize a porous carbon material with a Co–N_4 active site, followed by a series of MOF-derived porous carbon material oxygen reduction catalysts. Most of them are zeolitic imidazolate framework materials, mainly including ZIF-8 and ZIF-67, in which ZIF-8 pyrolysis products are N-doped nanoporous carbon, and ZIF-67 can obtain N-doped carbon nanotubes and other structures during pyrolysis, the ZIF-8-derived porous carbon has a large surface area, and the ZIF-67-derived porous carbon has an active Co–N site. Meng *et al.*[50] developed a simple and versatile method for synthesizing carbon nanotubes (CNTs) by prolonged pyrolysis of ZIF at low temperatures. Wang *et al.*[51] prepared a Co, N-doped carbon material (Co–N–CNT) by pyrolysis of 2D leaf-like ZIF-L. The ZIF-L precursor was synthesized by mixing a given amount of $Zn(NO_3)_2{\cdot}6H_2O$, $Co(NO_3)_2$ $6H_2O$ and 2-methylimidazole(2-MI), followed by direct pyrolysis under a 900 °C Ar atmosphere to obtain Co–N–CNT. Co–N–CNTs contain a large number of multi-walled carbon nanotubes up to several hundred nanometers. At the end of these multi-walled carbon nanotubes, crystallized cobalt nanoparticles are encapsulated (Fig. 6a). Interestingly, according to EDS analysis, N elements are only concentrated at the end of the carbon nanotubes containing cobalt nanoparticles (Fig. 6b), the presence of Co–NC sites was demonstrated, and the terminal structure completely exposed the Co–NC sites to the surface of the carbon nanotubes, which would enhance the electrocatalytic performance. If the Zn/Co ratio during the preparation of the precursor is changed, it can be observed that the derived resultants present different morphology from Co–N–CNTs. For pure Zn precursors, the final product is a nitrogen-doped carbon nanoribbon network (Fig. 6c). For pure Co precursors, the final product is a cobalt nanoparticle-loaded nitrogen-doped carbon nanosheet (Fig. 6d), the ORR catalytic activity ($E_{1/2}$ = 0.78 V, 0.72 V) of the two in 0.1 M KOH is also significantly lower than that of Co–N–CNTs ($E_{1/2}$ = 0.90 V), so the choice of precursor for the microscopic structure of the product is crucial.

N and Co doping is deemed to be a possible way to improve the ORR catalytic activity of the material. However, a large number of studies have shown that the Fe-containing catalyst sometimes exhibits higher activity than the Co-containing catalyst, so the doping of Fe into ZIF is also a common optimization method. Fe-Doped materials are also more likely to exhibit good ORR catalytic activity in acidic solutions, which are important for practical applications. Lai *et al.*[52] developed a new synthesis strategy of Fe–N/C materials, which is the construction of the ZIF-8 framework, Fe^{2+} ions were *in situ* introduced to the methanolic solution of Zn^{2+} and 2-MI to form

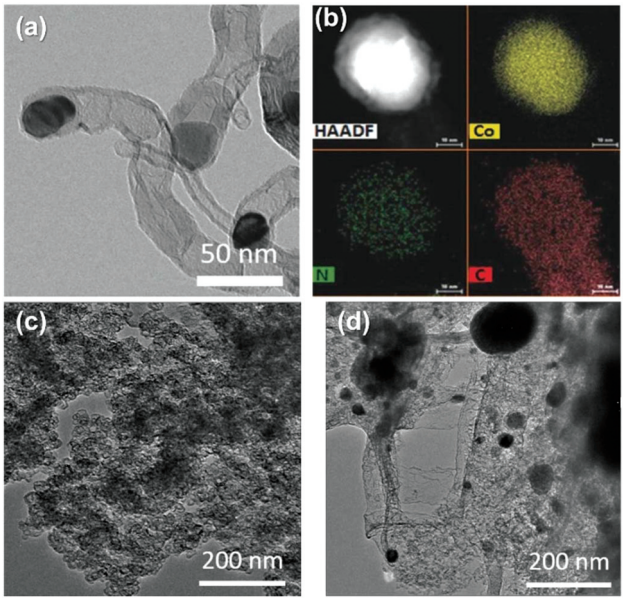

Fig. 6 (a) TEM image of Co–N–CNTs. (b) HAADF-STEM image and the corresponding EDS mapping of hybrid Co/Zn (1 : 1) ZIF-L-derived Co–N–CNTs, showing that N follows Co in the CNT networks. (c) TEM image of N-CNR derived Zn ZIF-L. (d) TEM images of Co/N–CNS derived Co ZIF-L.

uniform Fe-mIm NCs. The precursor is then pyrolyzed under a 900 °C Ar atmosphere, and Fe is converted into a highly active Fe–N_x site under the restriction of ZIF-8, instead of inactive inorganic phases such as metallic Fe or its carbides. A series of ZIF precursors 5% Fe–N/C, 10% Fe–N/C, 15% Fe–N/C, and 25% Fe–N/C can be obtained by adjusting the Zn^{2+}/Fe^{2+} molar ratio during the preparation of the precursor. When the iron content is gradually increased, the structure of the precursor changes from the polyhedral structure of ZIF-8 to the spherical structure of Fe-mlm. The ORR activity of the carbon derived from precursors (Fig. 7a) with different iron contents in 0.5 M H_2SO_4 solution showed that the catalytic activity of the material decreased gradually with the increase of iron content in the precursor, and $E_{1/2}$ is reduced from 5% Fe–N/C (0.735 V) to 25% Fe–N/C(0.610 V). The results of XPS (Fig. 7b) showed that the number of Fe–N_x sites on the surface of the material

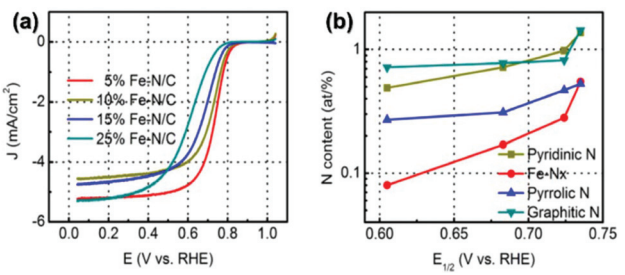

Fig. 7 (a) LSV curves in 0.5 M H_2SO_4 of Fe–N/C with different Fe contents in precursors. (b) The relationship between $E_{1/2}$ and different types of nitrogen contents.

decreased with the increase of Fe content in the precursor, and the EXAFS results showed that the coordination number of Fe atoms in the Fe–N_x site also decreased. Therefore, it can be concluded that a separate coordination structure of the Fe–N_x configuration will result in distinct electrocatalytic performance for the ORR, and different precursors will result in different site structures.

Furthermore, Wu *et al.*[53] finely regulated the proportion of iron doping in ZIF-8 according to the Mößbauer spectral data, determined the optimal iron doping ratio, and achieved complete atomic dispersion of FeN_4 sites. The prepared material has excellent catalytic activity.

As a research hotspot in recent years, single-atom catalysts (SACs) have unique advantages in terms of catalytic activity, and there are still many challenges in the preparation of single atoms. The MOF material has become an important precursor of single-atom catalysts owing to its possible precise control of metal atoms and its high porosity. Jiao *et al.*[54] mixed Fe-TCPP (TCPP = tetrakis (4-carboxyphenyl) porphyrin) and H_2-TCPP in a certain ratio to assemble a series of isomorphic MOF Fe_x-PCN-222 (x %: molar percentage of Fe-TCPP in both ligands), followed by pyrolysis. During the pyrolysis process, the 3D network of Fe_x-PCN-222 inhibits the aggregation of Fe atoms, and finally obtains the N-doped nanoporous carbon loaded with Fe atoms, which maintains the original rod-like structure and mesoporous characteristics of MOFs, and has excellent oxygen reduction activity and stability, half-wave potentials of 0.891 V and 0.776 V (*vs.* RHE) in 0.1 M KOH and 0.1 M $HClO_4$ respectively, and only 6 mV attenuation after 5000 cycles. Wang *et al.*[55] used an ultrasonic method to fix Fe^{3+} in the pores of the MOF, followed by pyrolysis. The Fe^{3+} moieties were decreased by as-generated carbon and bond with neighboring Co atoms, then catalyzing the graphitization of carbon, finally obtaining Fe–Co dual sites embedded in nitrogen-doped carbon. It exhibited excellent oxygen reduction activity, and the half-wave potential in the 0.1 M $HClO_4$ solution was 0.863 V (*vs.* RHE). In addition to pyrolysis of the MOF, Yin *et al.*[56] obtained Co single-atom/nitrogen-doped porous carbon (Co SAs/NC) by direct pyrolysis of Zn/CoZIF, where the addition of Zn enhances the distance between Co atoms. And there is an increase in N sites during pyrolysis, effectively suppressing the aggregation of Co atoms, thereby obtaining Co single-atom sites.

There are many studies on MOF composite derivatives as ORR catalysts. Guan *et al.*[57] used yolk-shell polystyrene@zeolitic imidazolate framework-67 (PS@ZIF-67) as a precursor to prepare single-holed cobalt/N-doped carbon hollow particles, and showed excellent ORR activity in 0.1 M KOH. Wang *et al.*[58] combined ZIF-8 crystals with NaCl to obtain ZIF-8@NaCl utilizing mechanical milling (Fig. 8). NaCl can serve as a limiting reactor during the pyrolysis process. Finally, ZIF-8@NaCl is pyrolyzed to obtain 3D nanosheet-linked polyhedral carbon (NLPC), which is defect-rich with a high N-doping level. For the 3D macroscopic structure, the initial potential was as high as 0.92 V in a 0.1 M KOH solution, which was close to that of Pt/C (0.94 V).

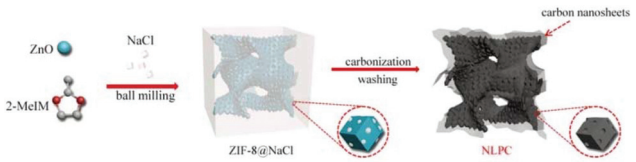

Fig. 8 The preparation of NLPC.

5. Molded carbon material-derived carbon-based catalyst

In recent years, a series of new carbon materials have become research hotspots, including fullerenes, graphene, carbon nanotubes, *etc*. Most of them have good electrical conductivity, a large specific surface area, a stable structure and an adjustable electronic configuration. Dodelet *et al.*[59] obtained microporous carbon-supported iron-based catalysts with high catalytic activity by mixing phenanthroline, iron and carbon carriers. Therefore, it is also a feasible solution to modify these molded carbon materials to obtain ORR catalysts,[60] and the pyrolysis method can effectively form sites with ORR catalytic activity on the surface of carbon materials, and thus is widely used. Ai *et al.*[61] used 2-aminothiophenol (ATP) as a source of N and S, and pyrolyzed a mixture of graphene oxide (GO) and ATP at 650 °C to obtain N, S co-doped graphene (NS-G). TEM images indicate that graphene sheets in NS-G randomly aggregate to form a porous NS-G cross-linking network. The close-to type IV N_2 adsorption–desorption isotherm with a clear hysteresis loop illustrates the coexistence of micropores (<2 nm) and mesopores (2–50 nm) in NS-G. This unique structural feature and the synergistic effect of N and S co-doping in graphene bring excellent electrochemical performance to NS-G. Ganesan *et al.*[62] pyrolyzed a mixture of cobalt thiourea and GO to prepare Cobalt sulfide nanoparticles dispersed on GO hybrids with ORR and OER bifunctionality. Zhang *et al.*[63] obtained an iron–nitrogen–carbon nanoparticle modified porous graphene (Fe–N–C/PGR) by pyrolysis of a complex of iron(II) phthalocyanine (FePc) nanoclusters and GO (Fig. 9). These studies have utilized the abundant oxygen-containing groups on the surface of the GO. The interaction between these oxygen-containing groups and the doping materials allows the doping materials to be uniformly fixed on the GO, and these interactions also contribute to pyrolysis. A site with ORR activity is established.

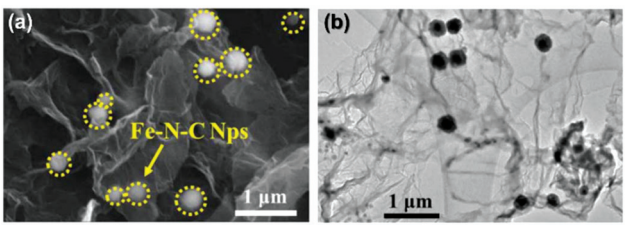

Fig. 9 (a) FESEM images of Fe–N–C/PGR (1 : 1) (b) TEM images of Fe–N–C/PGR (3 : 1) composites.

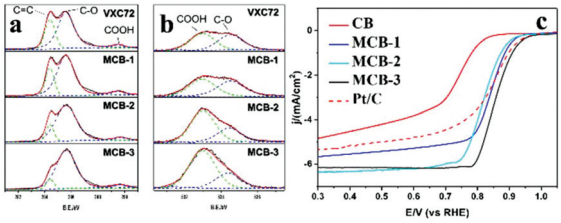

Fig. 10 (a) and (b) XPS survey spectra under synchrotron radiation and (a) high-resolution C1s scans of MCB-1, MCB-2, MCB-3 and the VXC72. (b) high-resolution O1s scan of MCB-1, MCB-2, MCB-3 and the VXC72. The dashed lines are the fitting peaks. (c) LSV curves of the MCB and other comparative catalysts in 0.1 M KOH.

The relatively defined chemical structure and electronic configuration of the shaped carbon material also provide a suitable material for studying the active sites of the ORR. Zhao *et al.*[64] introduced sp-N atoms into specific sites of few-layer oxidized graphdiyne (FLGDYO) by a pericyclic reaction. The presence of the sp-N site and its effect on ORR activity were subsequently analyzed.

Ni *et al.*[65] studied the process of modification of the surface of carbon black. Carbon black is a kind of loading material widely used in industry. It has good surface activity and electrical conductivity. Researchers adsorbed Co^{2+}, Zn^{2+} and 2-methylimidazole on the surface of carbon black[66] and then pyrolyzed it to obtain modified carbon black. Subsequent XPS and ORR results (Fig. 10) indicate that during modification of carbon black, a large amount of C=C was oxidized to C–O bonds on the surface of carbon black, and the catalytic activity of the materials is significantly enhanced with the increase of O content. This indicates that the C–O bond widely present in the pyrolytic carbon material can also serve as the active center of the ORR, which will be beneficial to the research of the inexpensive ORR catalyst and the explanation of the ORR mechanism.

6. Conclusions and perspectives

In summary, carbon based catalysts as the most promising NPMCs for the ORR have received extensive investigations during the last five years and significant progress has been made in this field. The pyrolysis method is one of the main methods for preparing carbon-based catalysts. This review provides a brief description of several typical carbon-based catalysts based on the classification of precursors and some analysis of the source of their activity. The sources of carbon-based catalysts are very extensive. Due to the large amount of organic matter in the biosphere, the research on organic matter is relatively deep. For the research of carbon-based catalysts, the ultimate goal is to obtain catalysts with low cost and excellent performance. Biomass-derived carbon materials have the widest source and the lowest price, but their performance is relatively poor, while the controllability is general, depending on the composition and structure of the biomass itself. The optimized space of the carbon material derived from the organic mixture is larger than the bio-carbon, so its performance is better than that of bio-carbon. However, the precursor mixture means that the composition and structure are not fixed. The amorphous pores brought by such precursors have certain influence on the catalytic activity. MOF-derived carbon materials largely inherit the characteristics of the original MOF and have many advantages, such as simple preparation procedures, framework structures, layered porous structures, large specific surface area, and convenient heteroatom doping schemes. It can be seen that the improvement in catalytic performance is from effective active sites, effective mass transfer and excellent stability of the matrix, which can be achieved by rational design and fabrication of MOF-derived carbon materials. So in the past period of time, MOF-derived carbon materials have made amazing progress. However, they still have problems such as high price, and further research is needed. Direct modification of the shaped carbon material can help us obtain a defined active site and help us to improve our understanding of the catalytic mechanism of the ORR.

In addition, some of the efforts to modulate the composition and geometry of the precursor to produce better performance are discussed. The composition of the precursor will significantly affect the structure of the pyrolysis product, the active site, and even the process of pyrolysis. For example, in the pyrolysis of ZIF, Zn can catalyze the graphitization of carbon, while Co can catalyze the formation of carbon nanotubes. Different Zn/Co ratios lead to completely different pyrolysis products. Similarly, the geometry of the precursor also has a huge impact on the pyrolysis products. The specific influence depends on the type of precursor. Generally, we hope that the elements in the precursor that may produce active sites are dispersed, so that the active sites will not lose their activity due to reunion. These rules can guide us to synthesize ORR catalysts in more efficient ways.

In addition to the activity optimization issues mentioned in this review, excellent durability under fuel cell operating conditions for practical applications is also important for carbon-based ORR catalysts, so the application of these high performance carbon-based catalysts to practical devices has a very long way to go which requires more scientists to invest in research.

Conflicts of interest

There are no conflicts to declare.

Acknowledgements

This work was supported by the National Key R&D Program of China (2017YFA0700101 and 2016YFA0202801) and the NSFC (21431003).

Notes and references

1 Y.-Z. Chen, R. Zhang, L. Jiao and H.-L. Jiang, *Coord. Chem. Rev.*, 2018, **362**, 1–23.

2 W.-J. Liu, H. Jiang and H.-Q. Yu, *Energy. Environ. Sci.*, 2019, **12**, 1751–1779.
3 R. Jasinski, *Nature*, 1964, **201**, 1212–1213.
4 X. Huang, Y. Wang, W. Li and Y. Hou, *Sci. China: Chem.*, 2017, **60**, 1494–1507.
5 L. Dai, Y. Xue, L. Qu, H.-J. Choi and J.-B. Baek, *Chem. Rev.*, 2015, **115**, 4823–4892.
6 L. Chong, J. Wen, J. Kubal, F. G. Sen, J. Zou, J. Greeley, M. Chan, H. Barkholtz, W. Ding and D.-J. Liu, *Science*, 2018, **362**, 1276–1281.
7 H. Nishihara and T. Kyotani, *Adv. Mater.*, 2012, **24**, 4473–4498.
8 D. S. Su, S. Perathoner and G. Centi, *Chem. Rev.*, 2013, **113**, 5782–5816.
9 J. A. R. van Veen and H. A. Colijn, *Ber. Bunsen-Ges.*, 1981, **85**, 700–704.
10 S. Gupta, D. Tryk, I. Bae, W. Aldred and E. Yeager, *J. Appl. Electrochem.*, 1989, **19**, 19–27.
11 C. Shang, M. Yang, Z. Wang, M. Li, M. Liu, J. Zhu, Y. Zhu, L. Zhou, H. Cheng, Y. Gu, Y. Tang, X. Zhao and Z. Lu, *Sci. China Mater.*, 2017, **60**, 937–946.
12 S. Wu, Y. Zhu, Y. Huo, Y. Luo, L. Zhang, Y. Wan, B. Nan, L. Cao, Z. Wang, M. Li, M. Yang, H. Cheng and Z. Lu, *Sci. China Mater.*, 2017, **60**, 654–663.
13 X. Ge, A. Sumboja, D. Wuu, T. An, B. Li, F. W. T. Goh, T. S. A. Hor, Y. Zong and Z. Liu, *ACS Catal.*, 2015, **5**, 4643–4667.
14 M. Hamdani, R. N. Singh and P. Chartier, *Int. J. Electrochem. Sci.*, 2010, **5**, 556–577.
15 T. Wang, J. Wang, X. Wang, J. Yang, J. Liu and H. Xu, *Sci. China Mater.*, 2018, **61**, 915–925.
16 M. Borghei, J. Lehtonen, L. Liu and O. J. Rojas, *Adv. Mater.*, 2018, **30**, 27.
17 S. Lu, Y. Jin, H. Gu and W. Zhang, *Sci. China: Chem.*, 2017, **60**, 999–1006.
18 L. Jiang, L. Sheng and Z. Fan, *Sci. China Mater.*, 2018, **61**, 133–158.
19 Q. Liu, Y. Wang, L. Dai and J. Yao, *Adv. Mater.*, 2016, **28**, 3000–3006.
20 D. Yan, L. Guo, C. Xie, Y. Wang, Y. Li, H. Li and S. Wang, *Sci. China Mater.*, 2018, **61**, 679–685.
21 P. Song, H. M. Barkholtz, Y. Wang, W. Xu, D. Liu and L. Zhuang, *Sci. Bull.Science Bulletin*, 2017, **62**, 1602–1608.
22 C. Zhao, G. Liu, N. Sun, X. Zhang, G. Wang, Y. Zhang, H. Zhang and H. Zhao, *Chem. Eng. J.*, 2018, **334**, 1270–1280.
23 X. Gao, X. Li, Z. Kong, G. Xiao and Y. Zhu, *Sci. Bull.*, 2018, **63**, 621–628.
24 E. Antolini, *Appl. Catal., B*, 2009, **88**, 1–24.
25 Y. J. Wang, D. P. Wilkinson and J. J. Zhang, *Chem. Rev.*, 2011, **111**, 7625–7651.
26 D. Higgins, P. Zamani, A. Yu and Z. Chen, *Energy Environ. Sci.*, 2016, **9**, 357–390.
27 J. Liu, E. L. Li, M. B. Ruan, P. Song and W. L. Xu, *Catalysts*, 2015, **5**, 1167–1192.
28 Y. M. Bar-On, R. Phillips and R. Milo, *Proc. Natl. Acad. Sci. U. S. A.*, 2018, **115**, 6506–6511.
29 J. Deng, M. Li and Y. Wang, *Green Chem.*, 2016, **18**, 4824–4854.
30 J. Lee, K.-H. Kim and E. E. Kwon, *Renewable Sustainable Energy Rev.*, 2017, **77**, 70–79.
31 S. Gao, K. Geng, H. Liu, X. Wei, M. Zhang, P. Wang and J. Wang, *Energy Environ. Sci.*, 2015, **8**, 221–229.
32 F. Pan, Z. Cao, Q. Zhao, H. Liang and J. Zhang, *J. Power Sources*, 2014, **272**, 8–15.
33 Q. Liu, C. Chen, F. Pan and J. Zhang, *Electrochim. Acta*, 2015, **170**, 234–241.
34 M. Graglia, J. Pampel, T. Hantke, T.-P. Fellinger and D. Esposito, *ACS Nano*, 2016, **10**, 4364–4371.
35 L. Zhao, *RSC Adv.*, 2017, **7**, 13904–13910.
36 S. Gao, H. Liu, K. Geng and X. Wei, *Nano Energy*, 2015, **12**, 785–793.
37 W. Wan, Q. Wang, L. Zhang, H.-W. Liang, P. Chen and S.-H. Yu, *J. Mater. Chem. A*, 2016, **4**, 8602–8609.
38 G. Liu, X. G. Li, J. W. Lee and B. N. Popov, *Catal. Sci. Technol.*, 2011, **1**, 207–217.
39 L. Wang, C. Yang, S. Dou, S. Wang, J. Zhang, X. Gao, J. Ma and Y. Yu, *Electrochim. Acta*, 2016, **219**, 592–603.
40 L. Cao, Z. Lin, J. Huang, X. Yu, X. Wu, B. Zhang, Y. Zhan, F. Xie, W. Zhang, J. Chen, W. Xie, W. Mai and H. Meng, *Int. J. Hydrogen Energy*, 2017, **42**, 876–885.
41 J. Li, Y. Zhang, X. Zhang, J. Huang, J. Han, Z. Zhang, X. Han, P. Xu and B. Song, *ACS Appl. Mater. Interfaces*, 2017, **9**, 398–405.
42 A. Serov, K. Artyushkova and P. Atanassov, *Adv. Energy Mater.*, 2014, **4**, 1301735.
43 Z. Pei, H. Li, Y. Huang, Q. Xue, Y. Huang, M. Zhu, Z. Wang and C. Zhi, *Energy Environ. Sci.*, 2017, **10**, 742–749.
44 P. Bogdanoff, I. Herrmann, M. Hilgendorff, I. Dorb, S. Fiechter and H. Tributsch, *J. New Mater. Electrochem. Syst.*, 2004, 7.
45 B. Tan, Z.-F. Wu and Z.-L. Xie, *Sci. Bull.*, 2017, **62**, 1132–1141.
46 M. Kuang, Q. Wang, P. Han and G. Zheng, *Adv. Energy Mater.*, 2017, **7**, 1700193.
47 X. Sun, A. I. Olivos-Suarez, D. Osadchii, M. J. V. Romero, F. Kapteijn and J. Gascon, *J. Catal.*, 2018, **357**, 20–28.
48 S.-N. Zhao, X.-Z. Song, S.-Y. Song and H.-j. Zhang, *Coord. Chem. Rev.*, 2017, **337**, 80–96.
49 S. Ma, G. A. Goenaga, A. V. Call and D. J. Liu, *Chemistry*, 2011, **17**, 2063–2067.
50 J. Meng, C. Niu, L. Xu, J. Li, X. Liu, X. Wang, Y. Wu, X. Xu, W. Chen, Q. Li, Z. Zhu, D. Zhao and L. Mai, *J. Am. Chem. Soc.*, 2017, **139**, 8212–8221.
51 T. Wang, Z. Kou, S. Mu, J. Liu, D. He, I. S. Amiinu, W. Meng, K. Zhou, Z. Luo, S. Chaemchuen and F. Verpoort, *Adv. Funct. Mater.*, 2018, **28**, 1705048.
52 Q. Lai, L. Zheng, Y. Liang, J. He, J. Zhao and J. Chen, *ACS Catal.*, 2017, **7**, 1655–1663.
53 H. Zhang, H. T. Chung, D. A. Cullen, S. Wagner, U. I. Kramm, K. L. More, P. Zelenay and G. Wu, *Energy Environ. Sci.*, 2019, **12**, 2548–2558.
54 L. Jiao, G. Wan, R. Zhang, H. Zhou, S.-H. Yu and H.-L. Jiang, *Angew. Chem., Int. Ed.*, 2018, **57**, 8525–8529.

55 J. Wang, Z. Huang, W. Liu, C. Chang, H. Tang, Z. Li, W. Chen, C. Jia, T. Yao, S. Wei, Y. Wu and Y. Li, *J. Am. Chem. Soc.*, 2017, **139**, 17281–17284.
56 Y. Peiqun, Y. Tao, W. Yuen, Z. Lirong, L. Yue, L. Wei, J. Huanxin, Z. Junfa, H. Xun, D. Zhaoxiang, Z. Gang, W. Shiqiang and L. Yadong, *Angew Chem., Int. Ed.*, 2016, **55**, 10800–10805.
57 B. Y. Guan, L. Yu and X. W. Lou, *Adv. Sci.*, 2017, **4**, 1700247.
58 Y. Wang, L. Tao, Z. Xiao, R. Chen, Z. Jiang and S. Wang, *Adv. Funct. Mater.*, 2018, **28**, 1705356.
59 M. Lefèvre, E. Proietti, F. Jaouen and J.-P. Dodelet, *Science*, 2009, **324**, 71–74.
60 J. Ma, Z. Xiang and J. Zhang, *Sci. China: Chem.*, 2018, **61**, 592–597.
61 W. Ai, Z. Luo, J. Jiang, J. Zhu, Z. Du, Z. Fan, L. Xie, H. Zhang, W. Huang and T. Yu, *Adv. Mater.*, 2014, **26**, 6186–6192.
62 P. Ganesan, M. Prabu, J. Sanetuntikul and S. Shanmugam, *ACS Catal.*, 2015, **5**, 3625–3637.
63 Y. Zhang, L. Qian, W. Zhao, X. Li, X. Huang, X. Mai, Z. Wang, Q. Shao, X. Yan and Z. Guo, *J. Electrochem. Soc.*, 2018, **165**, H510–H516.
64 Y. Zhao, J. Wan, H. Yao, L. Zhang, K. Lin, L. Wang, N. Yang, D. Liu, L. Song, J. Zhu, L. Gu, L. Liu, H. Zhao, Y. Li and D. Wang, *Nat. Chem.*, 2018, **10**, 924–931.
65 C. Ouyang, B. Ni, Z. Sun, J. Zhuang, H. Xiao and X. Wang, *Chem. Sci.*, 2019, **10**, 2118–2123.
66 N. Bing, O. Chen, X. Xiaobin, Z. Jing and W. Xun, *Adv. Mater.*, 2017, **29**, 1701354.